NASA Technical Memorandum 102603

APPLICATION OF VARIABLE-GAIN OUTPUT FEEDBACK FOR HIGH-ALPHA CONTROL

AARON J. OSTROFF

FEBRUARY 1990

National Aeronautics and Space Administration

Langley Research Center

Hampton, Virginia 23665

APPLICATION OF VARIABLE-GAIN OUTPUT FEEDBACK FOR HIGH-ALPHA CONTROL

Aaron J. Ostroff
NASA Langley Research Center
Hampton, Virginia

ABSTRACT

This paper describes a variable-gain, optimal, discrete, output feedback design approach that is applied to a nonlinear flight regime. The flight regime covers a wide angle-of-attack range that includes stall and post stall. The paper includes brief descriptions of the variable-gain formulation, the discrete-control structure and flight equations used to apply the design approach, and the high performance airplane model used in the application. Both linear and nonlinear analysis are shown for a longitudinal four-model design case with angles of attack of 5°, 15°, 35°, and 60°. Linear and nonlinear simulations are compared for a single-point longitudinal design at 60° angle of attack. Nonlinear simulations for the four-model, multi-mode, variable-gain design include a longitudinal pitch-up and pitch-down maneuver and high angle-of-attack regulation during a lateral maneuver.

INTRODUCTION

High angle-of-attack (α) flight is a desirable capability because of potentially large payoffs for combat aircraft. These airplanes will have to operate over a wide flight regime that includes stall and post stall. Post-stall technology (PST) fighters must therefore be capable of controlled flight beyond the maximum aerodynamic lift angle of attack. One goal is to make airplanes roll faster at high α, which drives up the pitch and yaw control power requirements. The problem is that the control power of conventional airplanes decreases as airspeed decreases. Research is under way on methods to improve controllability at high α where control power is low and departures most likely. One solution to the control power problem is the use of thrust vectoring controls. The use of thrust vectoring provides additional control power for stability augmentation as well as for maneuver enhancement in the stall and post-stall flight regimes.

The requirement for airplanes to operate with agility over a highly nonlinear flight regime puts additional burden on control law designers. A linear single-point design with constant feedback gains is probably inadequate to maintain good control properties over the complete α range. Typically, control designers develop satisfactory control laws at several points over the flight regime and then use an interpolation technique, often a least squares fit, to obtain final control gains. One potential problem with this approach is that the controller may lose performance characteristics and even stability, in high-order, highly-sensitive plants.

An objective of this research is to extend the operating range of the control law over the flight regime while continuing to use established linear control design and analysis techniques. In other words, the objective is to design a nonlinear control law using linear theory. The control methodology is an extension of previous developments for a direct-digital feedback design[1]. This paper describes the application of a variable-gain optimal output feedback control design methodology[2-4] in which the feedback gains are calculated and scheduled as a function of α. In general, several design parameters, either linear or nonlinear, may be used. Desired control characteristics are specified prior to designing the controller, negating the need for interpolation or gain-fitting techniques. Each of the operating points considered in the design contribute to the minimization of a global cost and are guaranteed to be stabilized.

The variable-gain formulation is discussed in the first section of this paper. Following this section is a description of a discrete control law structure that has been used successfully in other direct-digital design applications [5-8]. The third section includes a brief description of the airplane model used for this application. A section on the design example includes a description of four longitudinal linear design models and their associated linear analysis. In addition, linear time analysis for a single-point design is shown for comparison with nonlinear simulation results. The section on nonlinear simulation includes some practical aspects that must be considered, as well as single-point results and variable-gain scheduling results. Two different maneuvers are shown for the variable-gain scheduling example.

VARIABLE-GAIN FORMULATION

Variable-gain output feedback is an outgrowth of a stochastic, optimal, discrete, output feedback design approach for single-point control designs[1]. Typically, single-point designs are combined by using a curve fitting approach, such as a linear approximation or a higher-order least-squares fit. In contrast, the variable-gain approach [2-4] solves a control design problem by minimizing a performance index for an ensemble of systems. Equations describing the stochastic discrete output feedback system are functions of the argument, p, which in the general case represents various operating point parameters. The dynamic system, measurement and control law equations are

$$x(p,k+1) = \Phi(p)\, x(p,k) + \Gamma(p)\, u(p,k) + w(p,k) \quad (1)$$

$$y(p,k) = C(p)\, x(p,k) + \eta(p,k) \quad (2)$$

$$u(p,k) = -K(p)\, y(p,k) \quad (3)$$

where $\Phi(p)$, $\Gamma(p)$ and $C(p)$ represent the system matrices, $x(p,k)$, $y(p,k)$, and $u(p,k)$ are the state, measurement, and control vectors, $w(p,k)$ and $\eta(p,k)$ represent state process noise and sensor noise vectors, $K(p)$ is the feedback gain matrix and k is the sampling step. It is assumed that $w(p,k)$ and $\eta(p,k)$ are uncorrelated, zero-mean, white-noise vectors as

$$E[w(k,p)] = 0, \qquad E[\eta(k,p)] = 0 \tag{4}$$

$$E[w(k,p)\, w^T(j,p)] = W(p)\delta_{k-j} \tag{5}$$

$$E[(\eta(k,p)\eta^T(j,p)] = V(p)\delta_{k-j} \tag{6}$$

where W(p) and V(p) represent process-noise and sensor-noise covariance matrices, δ_{k-j} is the Kronecker delta and E is the expectation operator.

The feedback gain matrix has a linear functional relationship with the operating point parameters[2]

$$K(p) = K_O + \sum_{i=1}^{q} p_i\, K_i \tag{7}$$

It is not feasible to compute the gain K(p) for every possible variable (α, β, etc.) over an entire flight regime, so a selected set of p_i is used for the variable feedback-gain schedule. This selected set of parameters will be referred to as the variable-gain scheduled parameters in the remainder of this paper. Each of the p_i can be either linear or nonlinear, even though (7) shows a linear functional relationship between feedback gain and the gain-scheduled parameters. In the example design problem described in this paper, one gain-scheduled parameter that is a linear function of angle of attack (α), is used.

A quadratic performance index for the local discrete cost, $\bar{J}(p, K(p))$, of each plant described in (1) and (2) has the form

$$\bar{J}(p,K(p)) = \lim_{N\to\infty} \frac{1}{2(N+1)} \sum_{k=0}^{N} E[X(p,k+1)^T Q(p) X(p,k+1) + U(p,k)^T R(p) U(p,k)] \tag{8}$$

where $Q(p) \geq 0$, $R(p) \geq 0$ and X(p) and U(p) (to be described later) are augmented state and control vectors, respectively. A global cost is expressed by

$$J(K) = \sum_{j=1}^{M} f_j \bar{J}(p_j, K(p_j)), \quad f_j \geq 0 \tag{9}$$

where each of the local costs are summed and weighted, $f_j \geq 0$, to assign relative priorities to the individual plant models.

The main point of this variable-gain formulation is to find a variable feedback gain matrix, K(p), which minimizes the global cost (9) subject to the constraints defined in (1) - (7).

CONTROL LAW STRUCTURE

A PIF/CGT (proportional-integral-filter with command generator tracking) discrete controller structure is used for the control law[8,9]. PIF is a direct digital integrated formulation using linear dynamics for design. The controller inputs represent rate commands and the time step from rate to control position commands accommodate necessary computation delays. Proportional feedback of control position commands allows additional filtering within each control channel. Only measurable states are being fed back and selected outputs are being integrated to give type-1 control properties.

The PIF equations and weightings for the local cost function are formulated in the continuous domain and then transformed to the discrete domain. The discrete plant dynamics in (1) are augmented by additional dynamic equations as

$$u(p,k+1) = u(p,k) + (\Delta T)\, v(p,k) \tag{10}$$

$$z(p,k+1) = z(p,k) + (\Delta T)H_z\, x(p,k) + (\Delta T)D_z u(p,k) \tag{11}$$

where H_z and D_z are transmission matrices for the integrator states, z(p,k), v(p,k) is the control rate command and is used in equation (8) as U(p,k), and ΔT is the discrete sampling period. The PIF state vector, X(p,k), and output vector, Y(p,k), are defined as

$$X(p,k) = [x(p,k)^T,\, u(p,k)^T,\, z(p,k)^T]^T \tag{12}$$

$$Y(p,k) = [y(p,k)^T,\, u(p,k)^T,\, z(p,k)^T]^T \tag{13}$$

The PIF state vector X(p,k) is then used in the local cost equation (8).

The command generator uses an output model-following approach to achieve specific objectives, such as changes in pitch rate or angle of attack. Feedforward gains, connecting the command model to the control inputs, are calculated open loop, independent of the feedback gains. The objective of CGT is to cause selected outputs, y, of the airplane to track the output, y_m, of a linear command model using feedforward control theory. A more complete description is presented in reference 10 and chapter 4.10 of reference 9.

All equations are implemented in incremental form using total measurable quantities. This implementation has worked very well with nonlinear dynamics in other applications[5-7]. A significant advantage of this implementation is that it performs automatic trim. The airplane goes to a new equilibrium state as a function of slowly varying commands and, therefore, trim values are not needed in flight.

The main incremental flight control equations[8] are

$$v_k = T_u\, v_{k-1} + K_y(y_k - y_{k-1}) + T_i(y_{z,k-1} - y_{m,k-1}) + T_f(u_{m,k+1} - u_{m,k}) \tag{14}$$

$$u_{k+1} = u_k + (\Delta T)v_k \tag{15}$$

where y_z is the vector of integrated outputs, y_m is the output vector from the command model, u_m is the input vector to the command model, K_y is the feedback gain matrix associated with the plant outputs, and T_u, T_i, and T_f represent precomputed matrices. The control position command to the plant servo actuators is the vector u_k in equation (15).

AIRPLANE MODEL

The model used for this work has the characteristics of a high performance, high angle-of-attack (α) airplane that can undertake fighter or attack missions. For this study, the airplane has a gross weight of approximately 33,000 pounds, a wing span including tip missiles of 40 feet, and the length is 56 feet. Controls include two afterburner engines plus the following control surfaces (1) horizontal stabilators, (2) full-span leading-edge flaps, (3) trailing-edge flaps, (4) ailerons, and (5) twin vertical stabilizers. In addition, pitch and yaw thrust vectoring controls have been added for both longitudinal and lateral-directional maneuvering.

A nonlinear six degree-of-freedom, rigid-body dynamic model is used for batch simulations. The aerodynamic tables, generated from a wind tunnel derived data base, have an α range from -10° to 90° and a sideslip range of ±20°. Most coefficients are determined by using table lookup with linear interpolation. Flexibility effects are incorporated using flex/rigid ratios. During simulation, the aerodynamic control surfaces are driven by approximate transfer functions with constant rate and position limiting. Thrust vectoring actuator dynamics consist of a simple first-order low-pass filter for all four vanes, two for each engine, that provide pitch and yaw moments. Afterburner dynamics are included in the engine model, and engine thrust levels based upon airflow rate, which is determined by table lookup.

Table I shows the short period eigenvalues and trim Mach numbers for an α range from 5° to 60° at 15,000 feet. The airplane is trimmed straight and level up to α equal to 35 °; as α becomes larger, the flight path angle becomes negative. The reason is insufficient thrust is available at α greater than 35°. The data in Table I show that the short period open-loop eigenvalue becomes very lightly damped when α exceeds 40° (post-stall flight regime) with the airplane being slightly unstable for α at 50° and 55°. The phugoid (not shown) becomes more heavily damped as α increases.

The example application described in this paper includes the horizontal stabilator and thrust vectoring controls. The linear design assumes fourth-order dynamics for the stabilator (poles at -14.9 ± j33 and -62 ± j85) and first-order dynamics for the thrust vectoring control (pole at -30).

DESIGN EXAMPLE

Linear Design Model

Four flight conditions (α = 5°, 15°, 35°, and 60°) are used in the variable-gain output feedback application. The control law at these four flight conditions include two command modes with a transition region between these modes. A pitch rate, q-command, mode is used at low α (5°), whereas an α-command mode is used when α is 35° or higher. A transition region occurs between these two modes. The α-command is phased in between 5° and 15° of α and the q-command is phased out between 15° and 35° of α. This transition range may not be the optimum choice, but the example does demonstrate a practical capability to incorporate multi-mode design.

The airplane model used in the design example is discussed in the previous section. The plant has fourth-order longitudinal dynamics for the short period and phugoid modes, two controls with fifth-order actuator dynamics for the horizontal stabilator ,δ_s, and symmetric thrust vectoring ,δ_v, as well as three outputs for q, α, and n_z (normal acceleration). The n_z measurement is transmitted through a low-pass filter of 50 rad/sec, in order to make the measurement a function of one state as opposed to several states and controls. This additional filter gives a total of 10 states for the design plant.

The PIF controller used in this example has six states. Two of the states are created by feeding back the control position commands, which generates additional low-pass filtering. Two additional states are created by adding integrators to either q or α (depending on the mode) and to δ_v. The q or α integrator provides zero steady-state error for the commanded variable, while the δ_v integrator allows the thrust vectoring control to be maintained near zero-deflection or some other reference input. The final two controller states are created by second-order dynamic compensation to provide additional regulation of the short period mode. This compensation is designed by heavily weighting the error between the two dynamic compensator state outputs and the open-loop short period mode[6,11]. Outputs from all six controller states augment the three plant outputs, giving a total of nine feedback variables used in the variable-gain design example. The sampling period used is 0.31 seconds to correspond with an existing real-time simulation.

There are several possible gain scheduled parameters, p, that might be used for the variable feedback gain matrix (7), but since this controller is for high-α research, a gain schedule that is proportional to α has been selected. The function used is

$$p = \frac{\alpha - \alpha_o}{\alpha_o} \qquad (16)$$

where α_o is the reference value (5°) of the lowest α-trim case. Values of p for the four models used in the design are 0, 2, 6 and 11. Each of the models have equal weighting in the global cost (9).

Linear Analysis

Table II gives the s-plane, closed-loop eigenvalues and damping ratios for the four models. All closed-loop eigenvalues are computed in the z-plane (discrete), but are shown in the s-plane for simplicity. Each model corresponds to a flight condition as described in the previous section. The six most negative eigenvalues under model 1 correspond to actuator dynamics and the n_z filter. The closed-loop short period eigenvalues are at -3.19 ±j1.91, with a damping ratio of 0.86. The two eigenvalues nearest the origin represent the phugoid which has a reduced frequency and is more heavily damped than

the corresponding open-loop phugoid. The phugoid is not directly controlled, and the fact that the closed-loop phugoid is changed from the open-loop phugoid is due to coupling through the feedback measurements. The closed-loop, short period eigenvalues for models 2 through 4 are -0.96 ± j1.17, -0.79 ± j0.84, and -0.72 ± j1.04, respectively. Comparing all four models, the smallest damping ratio (excluding the phugoid and actuators) is 0.57 which is the short period mode for model 4. The open-loop damping ratio for the corresponding case is 0.004 (Table I). All other damping ratios are greater than 0.63. The controller (not shown) is completely stable except for one eigenvalue at the origin, due to the α or q integrator for each model.

Figure 1 contains the structured singular-value[12] for a multiplicative error when breaking the control loop for each model at the plant input (top plot) or the plant output (lower plot). The numbers on the curves refer to the model. The curve for model 1 is always above 1.0 for the plant input, and only goes below 1.0 at the lower frequencies for the plant output; the minimum is at 0.01 rad/sec, which is the closed-loop phugoid frequency. Model 2 results show minimum singular values slightly less than 0.9 (excluding the phugoid frequency which is very lightly damped) at both the plant input and the plant output. The lowest singular value at the plant input is slightly greater than 0.6 for model 4, and the lowest singular value at the plant output is approximately 0.48 for models 3 and 4. This last data indicates that a simultaneous diagonal perturbation at the plant output, as large as 48 percent, can insure stability at the frequency where the singular value is minimum.

The maximum singular value for the loop transfer is shown in figure 2. The top plot contains the singular values for all four models when the loop is broken at the plant input, and the bottom plot shows the singular values when the loop is broken at the plant output. The lightly-damped, open-loop phugoid frequency for models 1 to 3 are shown by the sharp peaks in the singular-value curves. The sharp peak in the curves for model 4 represent the open-loop short period which has a damping ratio of 0.004, whereas the open-loop phugoid for model 4 is highly damped at 0.61. The plots show that the crossover frequency at the plant input is less than 9 rad/sec for model 1 and less than 3 rad/sec for the other 3 models. All models show good attenuation characteristics at the high frequencies.

Prior to analyzing the variable-gain controller in a nonlinear simulation, single-point designs were developed to compare linear and nonlinear simulation results for maneuvers with large angle-of-attack excursions. Experience has shown that nonlinear simulation results should be similar to the linear simulation results, and gross differences between the two usually imply discrepancies in code or other anomalies in the nonlinear simulation. Figure 3 contains linear simulation plots for a point design at $\alpha = 60°$. This single-point design is different than the frozen variable-gain design point described previously for model 4. The only nonlinearity is a limiter that is inserted at the plant input to prevent unrealistic control commands. The top portion of figure 3 shows curves for α, q, θ, n_z, and y_m. A ramp signal ,y_m, with a slope of 1 rad/sec and a saturation of 1.0 rad is commanded. The α curve reaches the commanded value in approximately 3.2 sec, and then settles out to a steady-state error of approximately 0.1 rad. The reason for this error is due to the saturation of δ_s which is shown in the lower portion of figure 3 along with δ_v. The remaining control, δ_v, is normally commanded to zero degrees in steady-state, but δ_v levels out at a new steady-state value to help compensate for the saturation of δ_s. The two integrator errors for α and δ_v balance out, leaving each variable offset from the commanded value. There is approximately seven more degrees of operating range for δ_v, and a pilot could use this additional control to get α closer to the desired value. An equivalent nonlinear simulation for this single-point design, as well as nonlinear simulations of a variable-gain design, will be shown in the following section.

NONLINEAR SIMULATION

The airplane model and key features relating to the nonlinear batch simulation has been described previously. The nonlinear simulation has three controllers for the longitudinal, lateral and directional axes, respectively. The longitudinal controller was replaced initially with a fixed-gain controller based on a single-point design, and then the variable-gain longitudinal control law described in this paper. The lateral and directional controllers remained unchanged. An inertial coupling signal, normally included in the longitudinal controller to compensate for lateral-directional rotation rates, is not included in the simulations to be described. In the nonlinear simulation, variable-gain scheduling is used for all feedback gains, whereas linear interpolation is used for the feedforward gains.

Practical Aspects

Three practical aspects that should be considered are described in this section. The first is the need to use multi-mode controllers and to smoothly change modes during flight. As discussed previously under Design Example, two modes have been included in the variable-gain design with a transition between the modes.

The second consideration is to incorporate trim schedules in the nonlinear simulation. Linear designs are based upon flap and thrust levels for a particular trim case. In simulation, flap and thrust schedules are incorporated as a function of α to make the simulation perform as close as possible to the actual airplane. The schedules are shown in figure 4 as a function of time since this data is taken from one of the simulation runs. The five curves are α, leading and trailing-edge left flaps (DNL, DFL), power-lever angle command (PLAC), and thrust (TT). Units of the top four curves are degrees, and the bottom curve is in thousands of pounds. The thrust trim schedule is incorporated to simulate the action of a pilot who would normally push the throttle forward for increased thrust as the airplane pitches up. The open-loop thrust schedule is based upon the trim thrust (which is related to α) from the linear design. Notice that the thrust level lags the command by approximately 1 second.

A third practical consideration is a deadband nonlinearity in the δ_v control. Figure 5 shows the effective turning angle as a function of thrust vectoring deflection and nozzle area at an altitude of 15,000 feet. As an example, for a nozzle area of 320 square inches and a δ_v

deflection of 5°, there is no effective turning angle. The normal deadbands at the high-alpha cases considered are approximately ±6° out of a total range of ±25°. The approach used to help nullify this deadband effect is described later in this section. The thrust vectoring deadband has an effect on the control derivatives that are used for the linear designs. For cases where δ_v is trimmed to zero deflection, the deadband must be accounted for in all perturbations from trim. The δ_v control derivatives used in the linear designs described previously have been adjusted to compensate for this deadband.

Single-Point Results

Figures 6A and 6B illustrate nonlinear simulation results for the single-point design at $\alpha = 60°$, and should be compared with the linear time responses in figure 3. One main difference in figure 6 is that all angular units are in degrees. The command is a ramp input that starts at 0.2 sec and reaches the desired value at 1.2 sec. In figure 6A the airplane is trimmed at $\alpha = 35°$, and then commanded to reach an α of 60°. The α curve reaches 60° in approximately 3 seconds, has a slight overshoot, and then settles to the desired value. The bottom two curves in the figure ($\delta_{s,l}$ and $\delta_{v,l}$) represent the left stabilator and left thrust vectoring deflection controls. Although $\delta_{s,l}$ is approximately at the saturation level, there is enough power to maintain α at the desired value. The deadband adjustment can be seen in the $\delta_{v,l}$ curve. The effective thrust vectoring deadband is estimated as a function of nozzle area. This deadband is then added to the $\delta_{v,l}$ linear command to get the total δ_v command. As seen in the figure, δ_v is operating near zero deflection angle since it is not needed for this maneuver.

In contrast, figure 6B shows the same curves for an α-command of 90°. These results look more like the linear simulation results in figure 3. The alpha curve overshoots 90° and then settles at a steady-state error of 5° to 7°. $\delta_{s,l}$ is in hard saturation and $\delta_{v,l}$ is seen to peak at 15° and settle out at approximately 12°. There is much more thrust vectoring control left, and a pilot could easily use this control to increase α to the desired value.

Variable-Gain Results

Figures 7A and 7B illustrate the longitudinal variable-gain control using the four models described earlier in this paper. The curve labeled p represents the gain-scheduling parameter and the curve labeled ERROR represents the error between the command generator output, y_m, and the regulated variable (q or α). y_m initially represents a commanded q of 0 deg/sec and then changes to 60 deg/sec at 0.2 seconds. As α increases, the mode transitions to an α-command system and y_m represents 60° of α. At 8 seconds into the run, y_m commands α to decrease to 35°, and at 16 seconds, y_m reverts back to the initial command mode of 0 deg/sec for q.

The α curve starts at 5° trim and reaches 55° in less than 3.5 seconds, then slowly reaches the initial command of 60°. During this same time period the pitch attitude, θ, reaches 90°, with the flight path angle (not shown) peaking at 30° before dropping off. q reaches a peak of 40 deg/sec. At 8 seconds, α starts to decrease to the commanded values of 35°, reaching this value within 3 seconds with a slight overshoot. The final command shows α decreasing to the initial trim value of 5° approximately 3 seconds after the command is initiated. The q curve settles out to 0 deg/sec in steady-state. Both controls, $\delta_{s,l}$ and $\delta_{v,l}$, remain within the linear range. This contrasts with the single-point design where the stabilator saturates. With the exception of the initial transient response, $\delta_{v,l}$ operates near the deadband. The p curve has the shape of α, since the gain-schedule parameter is directly related to angle of attack. The ERROR curve represents the difference between the commanded value and the regulated variable, and is a function of the mode. Initially, ERROR is the difference between y_m and q. As α increases, ERROR becomes the difference between y_m and α. Finally, during the last 8 seconds of the simulation, ERROR is again the difference between y_m and q. Notice that ERROR goes to zero during all three steady-state periods.

The final set of plots, figures 8A and 8B, illustrate the ability of the variable-gain design to hold α while performing a lateral maneuver. This maneuver has similarities to a Herbst maneuver [13]. The longitudinal control shows y_m ramping from 0 deg/sec to 60° in 2 seconds. Seven seconds into the run, when α is 60° and θ slightly greater than 90°, a full lateral stick (PCA) is applied. The lateral command is maintained for 3 seconds as the airplane rolls about the velocity vector, illustrated by changes in Euler angles θ, ϕ, and ψ. At 11 seconds, PCA is returned to zero. At this time, there is a slight decrease in α, which then returns to the commanded value. After the rolling motion stops, the airplane nose pulls through negative θ and then heads to nose level. At the end of this maneuver, the airplane is heading in the opposite direction, holding α at 60° and with a negative flight path angle of -70°.

One important feature of the control approach can be observed from the curves $\delta_{v,c}$ (thrust vectoring symmetric command) and $\delta_{v,l}$. In the simulation, the longitudinal and lateral-directional thrust vectoring commands are summed prior to driving the control surfaces, with the longitudinal signal having priority. Excluding the initial transient while α is increasing, $\delta_{v,c}$ remains close to the deadband limits because of the integrator on the longitudinal thrust vectoring control command. During the

lateral maneuver, full thrust vectoring moments are applied by the lateral-directional controller to maximize roll rate because $\delta_{v,c}$ is maintained near zero deflection angle. A second benefit of maintaining $\delta_{v,c}$ near zero deflection angle is to reduce heating on the vanes by keeping them at the edge of the exhaust plume.

SUMMARY

An optimal variable-gain output feedback control approach has been described and applied to a highly nonlinear flight regime that includes stall and post stall. The variable-gain formulation takes advantage of linear control design techniques to develop a nonlinear control law. In contrast to the standard industry approach of scheduling feedback gains using either an interpolation technique or a least squares fit, the variable-gain methodology is a control design approach where a global cost is minimized as a function of selected design parameters. Each of the operating points considered in the design are guaranteed to be stable.

A discrete control structure is used in the application. The structure allows proportional feedback, integral feedback, and incorporates additional filtering by feeding back the control position commands that go to the plant. Additional dynamic compensation is also included to help regulate the short period mode. The controller used for this application is sixth order. The equations implemented in the nonlinear batch simulation are incremental and use total measurable quantities. Advantages of this formulation include automatic trim and subtraction of slowly varying biases in the measurements.

The airplane model has characteristics of a high performance, high angle-of-attack airplane. Thrust vectoring controls have been added to help stability augmentation and maneuverability in the post-stall flight regime. Aerodynamic data is available for the angle-of-attack range from -10° to 90°. Analysis of the open-loop short period mode indicates extremely low damping in the post-stall flight regime, and a few cases where the airplane is unstable.

The design approach is applied to four flight conditions (α = 5°, 15°, 35°, and 60°). A pitch rate command mode is used at low α, an angle-of-attack command mode is used at high α, with a transition region between the two modes. The design includes two controls (stabilator and thrust vectoring) and three measurements (q, α, and n_z). Closed-loop eigenvalue analysis of all four operating conditions (excluding actuator dynamics and the phugoid which is not directly controlled) show that the lowest damping ratio is 0.57 for the short period mode at α = 60°.

Comparison of linear and nonlinear time simulations for a single-point design at α = 60° show very similar results. Similarities include rise-time, overshoot and offset errors when one of the controls is saturated. Experience has shown that nonlinear simulation results should be similar to the linear simulation results, and gross differences between the two usually imply discrepancies in code or other anomalies in the nonlinear simulation.

Two maneuvers are illustrated for the variable-gain scheduling example. These maneuvers illustrate the smooth transition between modes, pitch-up and pitch-down capability, the ability of the controller to regulate at the commanded values with zero steady-state error, and the ability of the controller to hold a high α in the presence of lateral maneuvers. An important control feature is the ability to hold the thrust vectoring control near a commanded value (generally zero deflection), allowing maximum thrust vectoring capability for the lateral-directional system and helping to minimize heating of the vanes.

REFERENCES

1. Halyo, N.; and Broussard, J. R.: Investigation, Development, and Application of Optimal Output Feedback Theory - Volume I: A Convergent Algorithm for the Stochastic Infinite-Time Discrete Optimal Output Feedback Problem. NASA CR-3828, August 1984.

2. Halyo, N.; Moerder, D. D.; Broussard, J. R.; and Taylor, D. B.: A Variable-Gain Output Feedback Control Design Methodology. NASA Contract NAS1-17493. NASA CR-4226, March 1989.

3. Halyo, N.: A Variable-Gain Output Feedback Control Design Approach. Presented at the AIAA Guidance, Navigation, and Control Conference, Boston, MA. August 14-16, 1989.

4. Moerder, D. D.; Halyo, N.; Broussard, J. R.; and Caglayan, A. K.: Application of Precomputed Control Laws in a Reconfigurable Aircraft Flight Control System. ICS TM-86-102, Information and Control Systems, Inc., Hampton, VA. 1986.

5. Ostroff, A. J.; and Hueschen, R. M.: Reconfigurable Multivariable Control Law For Commercial Airplane Using A Direct Digital Output Feedback Design. NASA TM-85759, February 1984.

6. Ostroff, A. J.; and Hueschen, R. M.: Investigation of Control Law Reconfigurations to Accommodate a Control Element Failure on a Commercial Airplane. Presented at the 1984 American Control Conference, San Diego, CA. June 6-8, 1984.

7. Ostroff, A. J.: Techniques for Accommodating Control Effector Failures on a Mildly Statically Unstable Airplane. Presented at the 1985 American Control Conference, Boston, MA. 1985.

8. Broussard, J. R.: Design, Implementation and Flight Testing of PIF Autopilots for General Aviation Aircraft. NASA Contract NAS1-16303, Information and Control Systems Inc. NASA CR-3709, 1983.

9. Maybeck, P. S.: Stochastic Models, Estimation, and Control. Vol. 3, Academic Press, New York. 1982.

10. Broussard, J. R.; and O'Brien, M. J.: Feedforward Control to Track the Output of a Forced Model. IEEE Trans. Automatic Control, Vol. 25. August 1980, pp. 851-854.

11. Broussard, J. R.; and Halyo, N.: Active Flutter Suppression Using Optimal Output Feedback Digital Controllers. NASA Contract NAS1-16772, Information and Control Systems, Inc. NASA CR-165939, May 1982.

12. Doyle, John: Analysis of Feedback Systems With Structured Uncertainties. IEEE Proc., Vol. 129, Pt. D, No. 6. November 1982, pp. 242-250.

13. Herbst, W. B.: Future Fighter Technologies. Journal of Aircraft, Vol. 17. August 1980, pp 561-566.

Table I - Short Period Open-Loop

α	Mach	Eigenvalue	
		Real	Imag
5	.46	-.55	1.30
10	.33	-.37	.66
15	.28	-.28	.87
20	.26	-.25	.64
25	.24	-.25	.36
30	.22	-.24	.58
35	.20	-.27	.56
40	.19	-.27	.69
45	.19	-.033	.73
50	.19	.019	.83
55	.19	.023	1.17
60	.20	-.017	1.07

Table II - Closed-Loop Eigenvalues

MODEL 1

Real	Imag	Damping
−.622E+02	.857E+02	0.59
−.622E+02	−.857E+02	0.59
−.496E+02	.000E+00	1.00
−.301E+02	.000E+00	1.00
−.166E+02	.337E+02	0.44
−.166E+02	−.337E+02	0.44
−.158E+02	.000E+00	1.00
−.531E+01	.600E+01	0.66
−.531E+01	−.600E+01	0.66
−.319E+01	.191E+01	0.86*
−.319E+01	−.191E+01	0.86*
−.147E+01	.478E+00	0.95
−.147E+01	−.478E+00	0.95
−.155E+00	.000E+00	1.00
−.100E−01	.739E−02	0.80
−.100E−01	−.739E−02	0.80

MODEL 2

Real	Imag	Damping
−.621E+02	.852E+02	0.59
−.621E+02	−.852E+02	0.59
−.511E+02	.000E+00	1.00
−.306E+02	.000E+00	1.00
−.223E+02	.000E+00	1.00
−.153E+02	.333E+02	0.42
−.153E+02	−.333E+02	0.42
−.693E+01	.000E+00	1.00
−.461E+01	.372E+01	0.78
−.461E+01	−.372E+01	0.78
−.960E+00	.117E+01	0.63*
−.960E+00	−.117E+01	0.63*
−.862E+00	.000E+00	1.00
−.187E+00	.000E+00	1.00
−.117E−01	.133E+00	0.09
−.117E−01	−.133E+00	0.09

MODEL 3

Real	Imag	Damping
−.621E+02	.851E+02	0.59
−.621E+02	−.851E+02	0.59
−.517E+02	.000E+00	1.00
−.317E+02	.000E+00	1.00
−.280E+02	.000E+00	1.00
−.150E+02	.332E+02	0.41
−.150E+02	−.332E+02	0.41
−.498E+01	.370E+01	0.80
−.498E+01	−.370E+01	0.80
−.379E+01	.675E+00	0.98
−.379E+01	−.675E+00	0.98
−.791E+00	.841E+00	0.69*
−.791E+00	−.841E+00	0.69*
−.929E−01	.000E+00	1.00
−.566E−01	.177E+00	0.30
−.566E−01	−.177E+00	0.30

MODEL 4

Real	Imag	Damping
−.621E+02	.849E+02	0.59
−.621E+02	−.849E+02	0.59
−.507E+02	.000E+00	1.00
−.329E+02	.000E+00	1.00
−.285E+02	.000E+00	1.00
−.148E+02	.333E+02	0.41
−.148E+02	−.333E+02	0.41
−.886E+01	.106E+01	0.99
−.886E+01	−.106E+01	0.99
−.221E+01	.195E+01	0.75
−.221E+01	−.195E+01	0.75
−.720E+00	.104E+01	0.57*
−.720E+00	−.104E+01	0.57*
−.317E+00	.000E+00	1.00
−.204E+00	.432E−01	0.98
−.204E+00	−.432E−01	0.98

* Short period

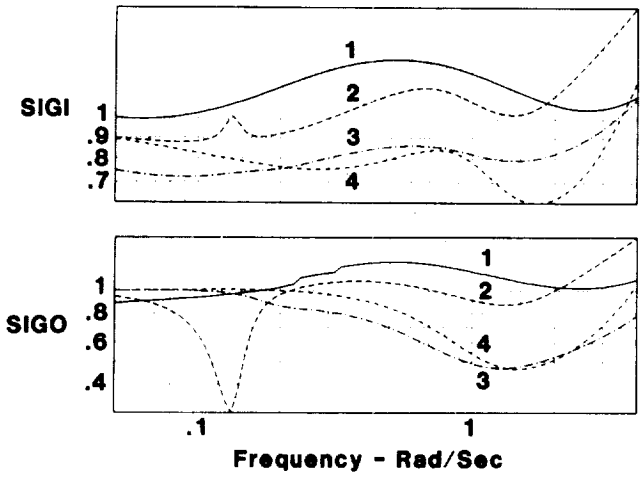

Figure 1.- Singular Value--Multiplicative Error.

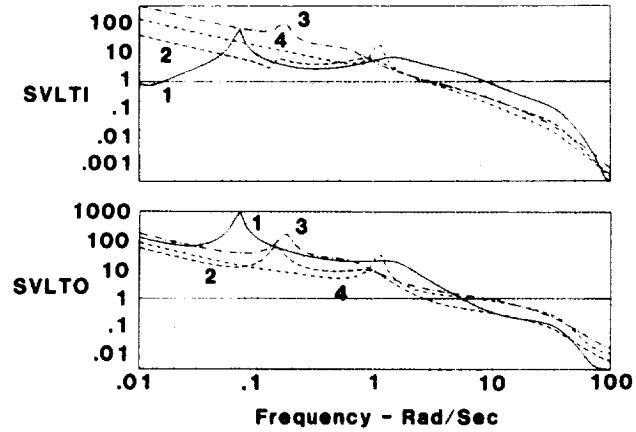

Figure 2.- Singular Value--Loop Transfer.

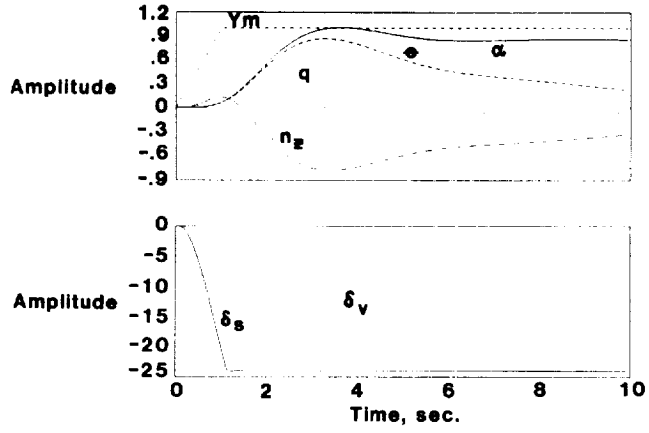

Figure 3.- Time Response for Design at 60°.

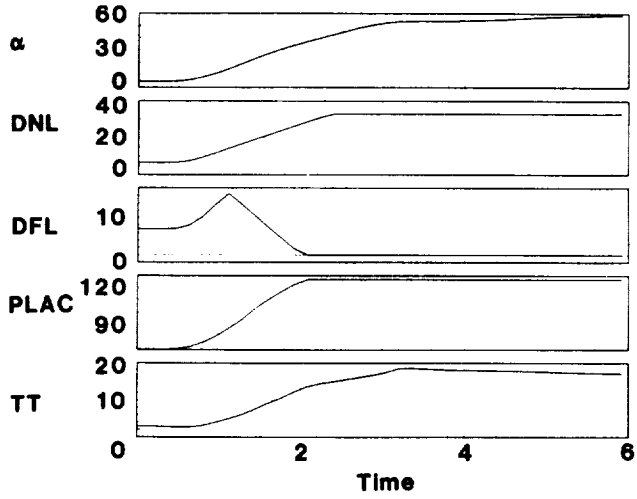

Figure 4.- Flap and Thrust Schedule.

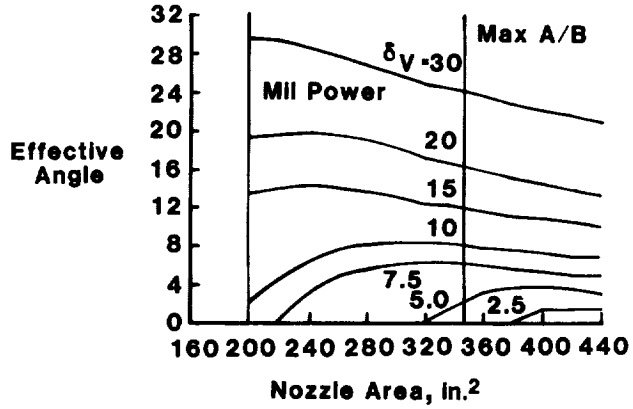

Figure 5.- Effective Turning Angle as a Function of Thrust Vectoring Deflection and Nozzle Area.

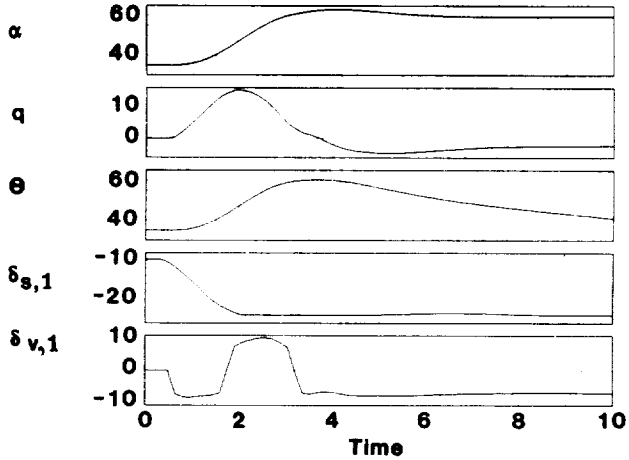

Figure 6a.- Two Independent Controls, Two Integrators, Alpha Command = 60.

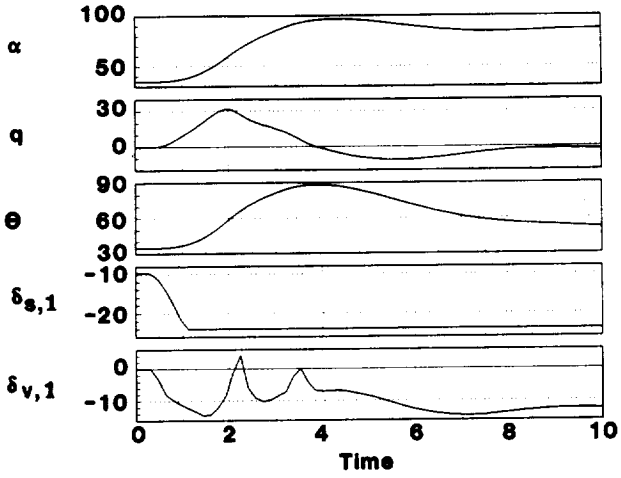

Figure 6b.- Two Independent Controls, Two Integrators, Alpha Command = 90.

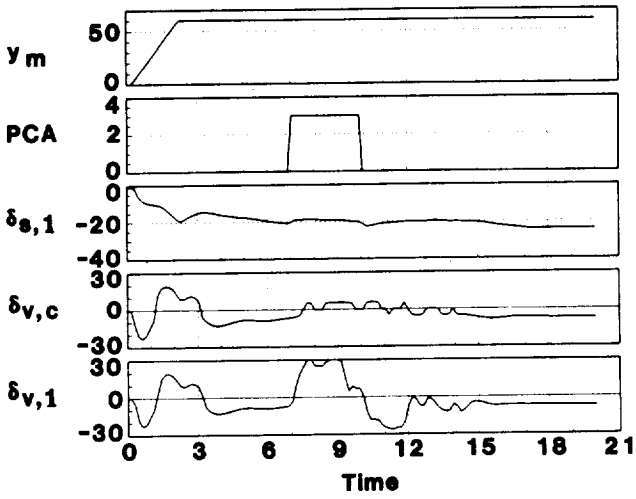

Figure 8a.- Variable Gain, Two Independent Controls, Lateral Stick, Four Models.

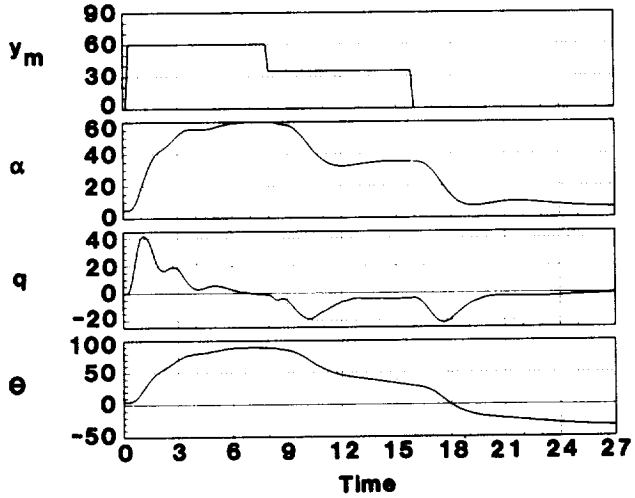

Figure 7a.- Variable Gain, Independent Controls, Four Models.

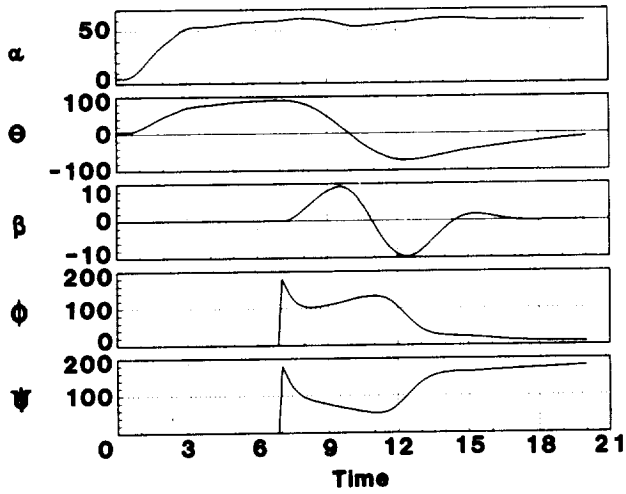

Figure 8b.- Variable Gain, Two Independent Controls, Lateral Stick, Four Models.

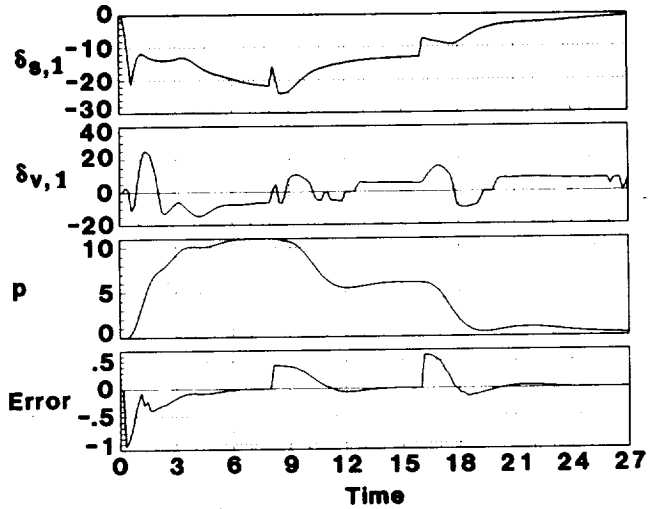

Figure 7b.- Variable Gain, Independent Controls, Four Models.

Report Documentation Page

1. Report No.	2. Government Accession No.	3. Recipient's Catalog No.
NASA TM-102603		

4. Title and Subtitle	5. Report Date
Application of Variable-Gain Output Feedback for High-Alpha Control	February 1990
	6. Performing Organization Code

7. Author(s)	8. Performing Organization Report No.
Aaron J. Ostroff	
	10. Work Unit No. 505-66-01-02

9. Performing Organization Name and Address	11. Contract or Grant No.
NASA Langley Research Center Hampton, VA 23665-5225	
	13. Type of Report and Period Covered
12. Sponsoring Agency Name and Address National Aeronautics and Space Administration Washington, DC 20546-0001	TECHNICAL MEMORANDUM
	14. Sponsoring Agency Code

15. Supplementary Notes

16. Abstract

This paper describes a variable-gain, optimal, discrete, output feedback design approach that is applied to a nonlinear flight regime. The flight regime covers a wide angle-of-attack range that includes stall and post stall. The paper includes brief descriptions of the variable-gain formulation, the discrete-control structure and flight equations used to apply the design approach, and the high performance airplane model used in the application. Both linear and nonlinear analysis are shown for a longitudinal four-model design case with angles of attack of 5°, 15°, 35°, and 60°. Linear and nonlinear simulations are compared for a single-point longitudinal design at 60° angle of attack. Nonlinear simulations for the four-model, multi-mode, variable-gain design include a longitudinal pitch-up and pitch-down maneuver and high angle-of-attack regulation during a lateral maneuver.

17. Key Words (Suggested by Author(s))	18. Distribution Statement
controls variable-gain output feedback high angle of attack superagility	UNCLASSIFIED - UNLIMITED Subject Category 08

19. Security Classif. (of this report)	20. Security Classif. (of this page)	21. No. of pages	22. Price
UNCLASSIFIED	UNCLASSIFIED	10	A02